


SCIENTIFIC REPORTS



OPEN

A synthetic combinatorial approach to disabling deviant Hedgehog signaling

C.-W. Fan¹, N. Yarravarapu¹, H. Shi², O. Kulak¹, J. Kim³, C. Chen² & L. Lum^{1,4} 

Mutations in components of the Hedgehog (HH) signal transduction pathway are found in the majority of basal cell carcinoma (BCC) and medulloblastoma incidents. Cancerous cells with intrinsic or acquired resistance to antagonists targeting the seven transmembrane effector Smoothened (SMO) frequently invoke alternative mechanisms for maintaining deviant activity of the GLI DNA binding proteins. Here we introduce a chemical agent that simultaneously achieves inhibition of SMO and GLI activity by direct targeting of the SMO heptahelical domain and the GLI-modifying enzymes belonging to the histone deacetylase (HDAC) family. We demonstrate a small molecule SMO-HDAC antagonist (IHR-SAHA) retains inhibitory activity for GLI transcription induced by SMO-dependent and -independent mechanisms frequently associated with cancer biogenesis. Synthetic combinatorial therapeutic agents such as IHR-SAHA that a priori disable cancer drivers and anticipated mechanisms of drug resistance could extend the duration of disease remission, and provide an alternative clinical development path for realizing combinatorial therapy modalities.

Cellular response to the secreted HH proteins is initiated upon their binding to the multi-pass protein Patched 1 (PTCH1), a suppressor of the seven transmembrane receptor Smoothened (SMO)¹. Activated SMO promotes SUFU disassociation from the GLI DNA binding proteins thus licensing them for gene transcriptional activation^{2,3}. Deviant HH pathway activity associated with several cancers including medulloblastoma (MB) and basal cell carcinoma (BCC) is commonly induced by mutations in *PTCH1*^{4,5}. SMO antagonists that are FDA-approved for the management of metastatic BCC (Vismodegib and Sonidegib) are able to restore homeostatic levels of signaling and blunt tumor growth⁶.

Despite an impressive initial response in some metastatic BCC patients, durable tumor growth suppression by SMO antagonists has been elusive and few treatment options that are available to patients after progression. Yet, the majority of the tumors that re-emerge are likely to be still dependent upon GLI transcriptional activity as determined by the appearance of mutations in SMO that prevent drug binding^{7–11}, kinase-dependent mechanisms promoting sustained GLI activity in the absence of SMO input^{12,13}, or *GLI2* gene amplification^{8,14}. Thus, agents that disrupt GLI activity have broader indications than those targeting SMO in HH-associated cancers particularly in cases of drug resistance.

A number of strategies for disrupting GLI activity have been evaluated including those that promote GLI protein turn-over such as arsenic trioxide^{15,16} or GANT61¹⁷, instigate SUFU activity (ABT-199)¹⁸, or have limited mechanistic accounting¹⁹. The activity of GLI proteins also appear to be blunted by their acetylation thus offering opportunities for disabling GLI activity by blocking GLI deacetylases²⁰. This strategy appears to be useful in blocking the growth of medulloblastomas in preclinical models of the disease²¹.

We had previously described a symmetric molecule with potent SMO inhibitory activity called IHR-1²². During the course of generating a fluorophore-labeled probe for visualizing IHR-1 interaction with SMO, we identified an active intermediate containing a long aliphatic linker that retained similar activity to the parental compound. We recognized that with an additional chemical step one could install the histone deacetylase

¹Department of Cell Biology, University of Texas Southwestern Medical Center, Dallas, TX, 75390, USA. ²Department of Biochemistry, University of Texas Southwestern Medical Center, Dallas, TX, 75390, USA. ³Department of Internal Medicine, University of Texas Southwestern Medical Center, Dallas, TX, 75390, USA. ⁴Present address: Pfizer Worldwide Research and Development, 10724 Science Center Drive, La Jolla, CA, 92121, USA. C.-W. Fan and N. Yarravarapu contributed equally to this work. C. Chen and L. Lum jointly supervised this work. Correspondence and requests for materials should be addressed to C.C. (email: chuo.chen@utsouthwestern.edu) or L.L. (email: Lawrence.lum@utsouthwestern.edu)

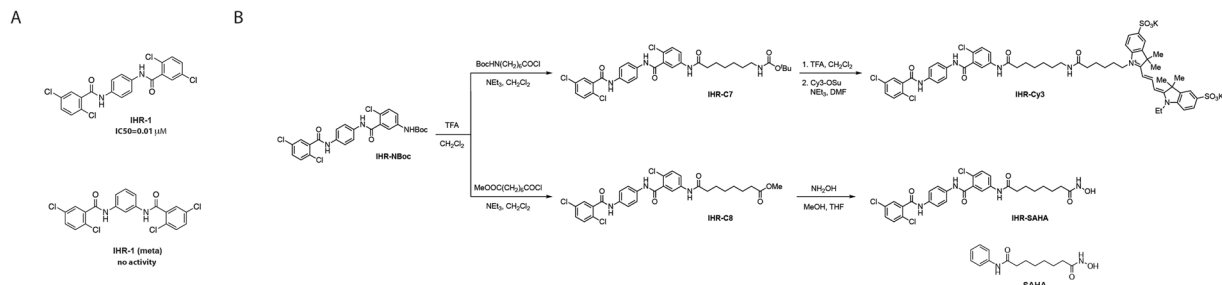


Figure 1. The origin of IHR-SAHA, a fusion molecule with potentially dual cellular activities. **(A)** Structures of IHR-1 and the inactive variant IHR-1 (meta)²². **(B)** The synthesis of IHR-Cy3 and IHR-SAHA. IHR-Cy3 is a chemical probe for monitoring IHR-1 interaction with SMO. Its synthetic intermediates IHR-NBoc and IHR-C7 retain anti-SMO activity (see Supplementary Fig. S1). The C7-amide moiety of IHR-C7 resembles SAHA and inspired the development of IHR-SAHA. The structure of SAHA is also shown.

(HDAC)-inhibitory pharmacoperones found in suberanilohydroxamic acid (SAHA, also known as Vorinostat) to potentially generate a dual antagonist. Here we characterize the mechanism of action for this molecule called IHR-SAHA that supports HH pathway inhibitory activity.

Results

Generation of a SMO-HDAC antagonist. The symmetric IHR-1 compound is a potent SMO antagonist identified from screening a diverse synthetic chemical library (Fig. 1A)²². Similar to other SMO antagonists, IHR-1 targets the heptahelical bundle to presumably promote an inactive conformation thus rendering cells HH-unresponsive. In addition, we had previously shown that the SMO inhibitory activity of IHR-1 is lost by switching the substitution pattern from *para* to *meta* (see Fig. 1A)²². The path to generating a fluorescent probe used for measuring IHR-1 binding to SMO (IHR-Cy3) entailed first replacing a chlorine atom of IHR-1 with an amino group followed by the addition of an aliphatic extension used to bridge Cy3 to IHR-1 (IHR-C7; Fig. 1B, Supplementary Fig. S1)²². The retention of anti-SMO activity in IHR-Cy3 suggests that chemical adducts with other cell biological activities in place of Cy3 could be engineered into this backbone²². To test this hypothesis, we created an IHR-1 derivative that now incorporates a molecule resembling the HDAC inhibitor SAHA (see Fig. 1B).

IHR-SAHA retains HDAC inhibitory activity. To determine if the addition of IHR-1 to SAHA altered its inhibitory profile amongst HDAC family members, we performed *in vitro* IC₅₀ assays against purified HDAC proteins (Fig. 2; Supplementary Table S1). Comparing these results with those previously generated using the same assay conditions and reagents²³, we observed a similar activity profile suggesting that the addition of IHR-1 did not significantly change the selectivity of SAHA for class I and II HDAC family members (see Fig. 2). Based on the outcome of studies focused on the major HDAC classes known to be inhibited by SAHA²⁴, we assume differences in any biological activity between SAHA and IHR-SAHA are not likely to be greatly impacted by alterations in the selectivity of HDAC inhibition.

SMO and HDAC inhibitory activities in IHR-SAHA are modular. To determine if the activity of the anti-SMO or anti-HDAC warheads is influenced by their chemical linkage, we generated an IHR (meta)-SAHA molecule which presumably would allow us to evaluate the anti-HDAC activity of IHR-SAHA in the absence of anti-SMO activity (Fig. 3A). Inactivation of the anti-SMO activity in IHR (meta)-SAHA did not affect the ability of IHR (meta)-SAHA to block nuclear HDAC activity as evidenced by the accumulation of acetylated-histone 3 (Ac-H3) suggesting that the two chemical activities are uncoupled (Fig. 3B). In addition, IHR (meta)-SAHA retains the ability to block SHH-induced GLI activity despite not possessing anti-SMO activity when evaluated using a cell based reporter assay of HH signaling (Fig. 3C).

IHR-SAHA exhibits activity against drug-resistant drivers of GLI activity. We next examined the activity of IHR-SAHA against three cancer-related genetic alterations known to induce deviant GLI activity (Fig. 4A–C). Loss of *Ptch1* is associated with ~70% of BCCs and 45% of SHH-subtyped medulloblastomas whereas the SMO mutations (such as the constitutively active SMO-M2 [W535L] mutation) is less frequently found in these diseases^{4,5}. SMO-L412F is an acquired SMO mutation that alters the drug-binding pocket in the heptahelical domain¹⁴. In cells with loss of *Ptch1*, IHR-SAHA exhibited slightly improved levels of activity against SMO-driven GLI activity compared with IHR-1 perhaps due to the attachment of SAHA to IHR-1. However, in cells expressing SMO-M2 or SMO-L412F which are intrinsically resistant to SMO antagonists²⁵, IHR-SAHA exhibited a much greater activity compared to IHR-1. The different activity of IHR-1 and IHR-SAHA in the two contexts (*Ptch1* null and SMO activating mutations) could be explained by an increase in cell permeability of IHR-SAHA compared with IHR-1 (Supplementary Fig. S2) and the previously described rogue activity of SMO-M2 and SMO-L412F from an intracellular compartment that renders cell impermeable SMO antagonists less active²². In the case of *Ptch1* null cells, IHR-1 and IHR-SAHA exhibit similar ability to block GLI transcriptional activity due to SMO signaling activity from the primary cilium and not an intracellular component. We also more directly evaluated the effectiveness of IHR-SAHA to disable deviant GLI activity in cells harbor a *GLI*

Class	HDAC	IHR-SAHA IC ₅₀	SAHA IC ₅₀
I	HDAC1	285 nM	41 nM
	HDAC2	746 nM	66 nM
	HDAC3	188 nM	41 nM
	HDAC8	>10 μ M	>2 μ M
IIa	HDAC4	>10 μ M	>10 μ M
	HDAC5	>10 μ M	>10 μ M
	HDAC7	>10 μ M	>10 μ M
	HDAC9	>10 μ M	>10 μ M
IIb	HDAC6	47 nM	18 nM
	HDAC10	174 nM	58 nM

Figure 2. IHR-SAHA retains similar specificity for SAHA-targeted HDACs. Activity profile of IHR-SAHA against different classes of HDACs was evaluated using an *in vitro* deacetylation assay. Each data point used to generate the IC₅₀ curve is an average of duplicate experiments (see Supplementary Table S1). SAHA activity in the same assay platform from a reference dataset is provided.

gene amplification (Fig. 4D). We observed anti-GLI activity with both IHR-SAHA and IHR (meta)-SAHA in RMS13 cells, which exhibit GLI-BS reporter activity as a consequence of *GLI1* amplification. We noted that SAHA appeared to be weaker in activity in this cell line compared to the IHR-SAHA or IHR (meta)-SAHA fusion molecules suggesting that the IHR-1 and IHR-1 (meta) adduct somehow improved SAHA activity in cultured cells.

IHR confers increased HDAC activity to SAHA. Consistent with increased activity of IHR-SAHA and IHR (meta)-SAHA fusion molecules compared with SAHA for inhibiting GLI activity seen in RMS13 cells which harbor *GLI1* amplification, we observed a similar trend for these molecules when using acetylated tubulin accumulation as a readout of SAHA activity (Fig. 5). Thus, the presence or absence of anti-SMO in the chemical agent does not appear to explain the increase in anti-HDAC activity seen in IHR-SAHA and IHR (meta)-SAHA (see Fig. 5). HDAC6, a target of SAHA, regulates the abundance of acetylated tubulin^{26,27}. Though not evaluated here, the addition of IHR-1 may have increased the cell permeability of SAHA (just as SAHA may have increased the cell permeability of IHR-1) given that both IHR-SAHA and SAHA appear to exhibit similar activities against recombinant HDAC6 *in vitro* (see Fig. 2).

IHR-SAHA prevents GLI binding to DNA. Whereas GLI1 acetylation has previously been shown to be sensitive to a chemical inhibitor of HDACs, the effect of such compounds on GLI binding to DNA has not been interrogated²⁰. We developed an *in vitro* assay that would allow us to monitor the effects of IHR-SAHA on GLI1 interaction with DNA (Fig. 6A). Monitoring endogenously expressed GLI1 protein in RMS13 cells, we observed loss of GLI1 binding to solid-support immobilized oligos harboring a consensus GLI binding sequence in the presence of SAHA and IHR-SAHA but not IHR-1 (Fig. 6B). Thus, the acetylation status of GLI proteins likely influences their ability to bind DNA and to regulate transcription of HH-controlled target genes.

Discussion

A testament to the growth-promoting prowess of GLI proteins in certain cancer types such as basal cell carcinoma and medulloblastoma is the continued reliance of cancerous cells resistant to SMO antagonists on GLI activity⁵. A number of strategies to counter the emergence of drug resistance have been proposed including those targeting PI3K^{8,13,28,29} or atypical protein kinase C ι/λ (aPKC- ι/λ)¹² which promote GLI activity even in the absence SMO signal, or inducing SUFU activity by removing the suppressive interaction of cytosolic prosurvival BCL-2 family members with SUFU¹⁸. A priori treatment with dual pathway antagonists such as the one described here may delay the emergence of drug resistance facilitated by these previously observed mechanisms. We also note that a similar strategy to the one described here has been reported albeit this case using the SMO antagonist Vismodegib as a scaffold³⁰ or as a drug combination³¹. Vorinostat is FDA-approved for the treatment of cutaneous T cell lymphoma, but so far has shown a more limited response in solid tumors³². Given the contribution of HH signaling in some of these diseases, there may be indications for the use of IHR-SAHA in cancers not routinely sequenced for mutations in known HH pathway components.

The improvements in activity of both IHR-1 and SAHA from their chemical fusion reinforce a lesson learned from our previous study that the activity changes associated with altered intrinsic cell membrane permeability

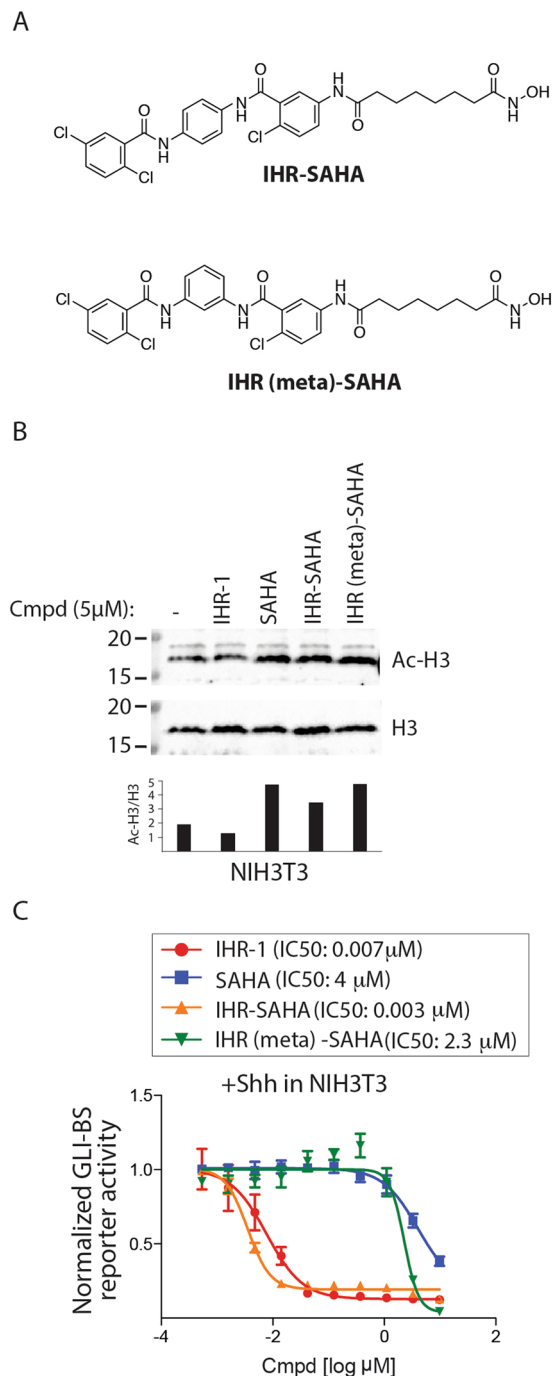


Figure 3. Anti-SMO and -HDAC activities in IHR-SAHA are modular. **(A)** Structures of IHR-SAHA and IHR (meta)-SAHA. IHR (meta)-SAHA is a fusion of IHR-1 (meta) and SAHA. **(B)** IHR-SAHA and IHR (meta)-SAHA retain HDAC inhibitory activity as measured by Western blotting for acetylated histone 3 (Ac-H3) in NIH-3T3 cells. The ratio of Ac-H3 to total H3 was quantified. Unprocessed blots are found in Supplementary Fig. S3. Two independent experiments were performed. **(C)** IHR-SAHA and IHR (meta)-SAHA exhibit different levels of anti-HH pathway activity. Indicated compounds were evaluated for their activity using a HH pathway reporter (GLI-BS reporter). Pathway response is reported as the ratio of Gli-BS and control reporter activities. Data show the mean and SD of three samples. Two independent experiments were performed.

of chemical probes could be exploited for understanding the subcellular site-of-action for protein queries²². The addition of SAHA likely increased the cell membrane permeability of IHR-1 as has been seen with other IHR-1 derivatives that improves its ability to target intracellularly localized SMO-M2 and SMO-L412F²² and with cell permeability studies using a molecule similar to IHR-SAHA (see Supplementary Fig. S2). We also acknowledge that differences in the cell membrane permeability of these molecules are not mutually exclusive from hypotheses that include IHR-SAHA inhibiting SMO mutants in a manner distinct from that of IHR-1 alone, or that

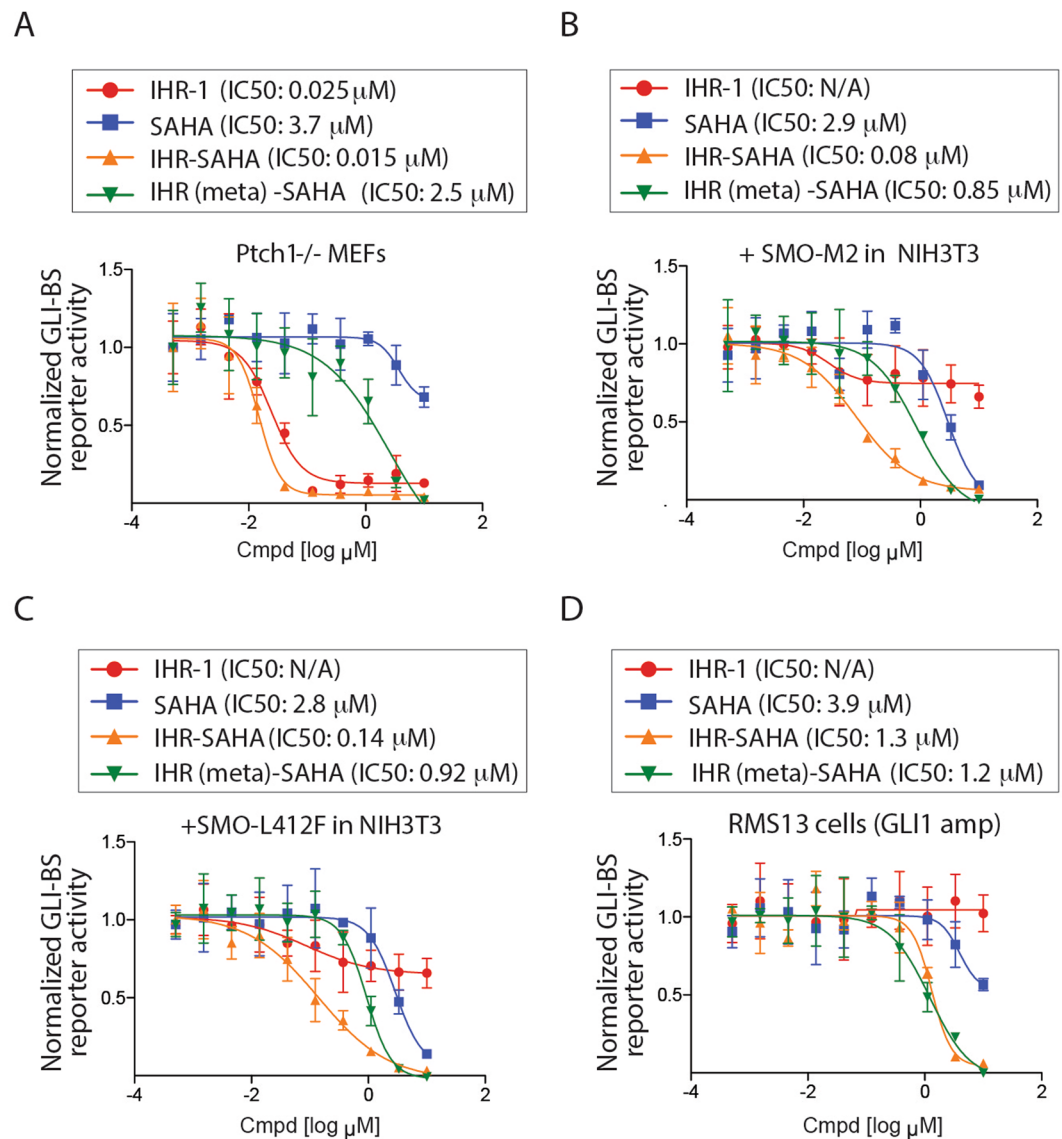


Figure 4. Activity of IHR-SAHA against drug resistance forms of HH signaling. GLI-BS and control reporter were transfected into *Ptch*^{-/-} MEFs (A), NIH3T3 cells with SMO-M2 DNA (B) or SMO-L412F DNA (C), or RMS13 cells which harbor *GLI1* gene amplification (D). Pathway response is reported as the ratio of Gli-BS and control reporter activities. Data show the mean and SD of three samples. Two independent experiments were performed.

IHR-SAHA simply inhibits SMO heptahelical domain more potently than unmodified IHR-1. Regardless of the mechanism, the observed increased inhibition of SMO and HDACs with IHR-SAHA when compared with either individual IHR-1 or SAHA that may correlate with improvements in the *in vivo* activity of both molecules as a consequence of their chemical fusion.

HDAC1 and HDAC6 activities are inhibited by IHR-SAHA at a nanomolar range *in vitro*. Whereas HDAC1 inhibition has been shown to directly affect GLI acetylation²⁰, genetically based elimination or chemical inhibition of HDAC6 with selective small molecules is sufficient to block a subset of GLI transcriptional targets and SMO-M2-driven medulloblastoma growth *in vivo*³³. In addition, HDAC6 inhibitors modulate primary cilium stability, an organelle that facilitates the relinquishing of SUFU suppression^{3,34} and proteolytic processing of GLI3 into a transcriptional repressor³⁵⁻³⁹. Thus, IHR-SAHA could impact GLI activity directly by targeting HDAC1 and indirectly by altering aspects of primary cilium function.

In addition to the cancer biology and medicinal chemistry considerations that may argue for a utility of multi-targeting agents in cancer management, there may also exist advantages for such a strategy in clinical development stages. For phase I studies with two drug combinations, optimal dose schedules for each drug need to be identified through formal dose escalation studies⁴⁰ where the concentration of one drug is increased at various fixed concentrations of the other drug. These studies require several treatment arms, larger number of patients and increased time compared to single drug phase I studies. Furthermore, pharmacokinetics of each drug will

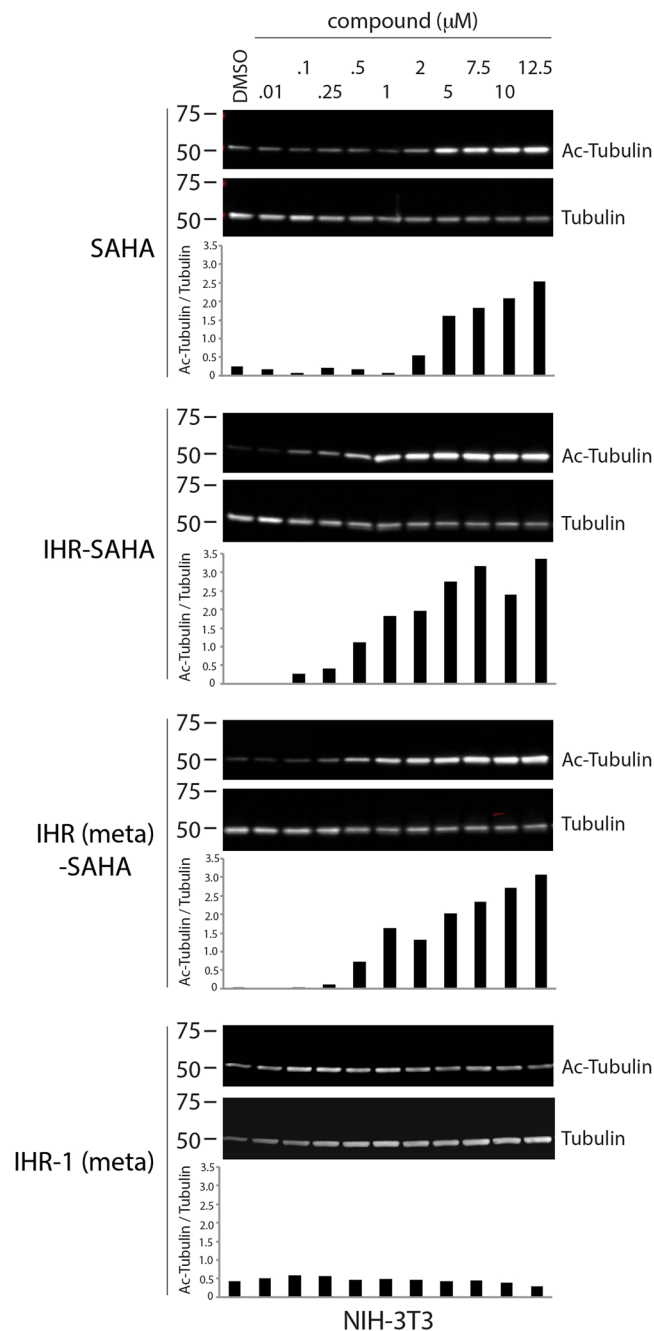


Figure 5. IHR-SAHA compounds exhibit increased HDAC inhibitory activity compared to SAHA. Abundance of total or acetylated tubulin was determined by Western blot analysis of NIH-3T3 cells treated with indicated concentrations of compound. The ratio of acetylated tubulin to total tubulin was quantified for each condition. Unprocessed blots are found in Supplementary Fig. S3. Two independent experiments were performed.

need be monitored as the drug-drug interactions may alter their metabolism and bioavailability⁴⁰. With single fusion compounds, such as IHR-SAHA, the dose of each drug component is fixed thus requiring a simple dose escalation study and only the single fusion compound need to be monitored for pharmacokinetics. Thus, fusion compounds can potentially accelerate and simplify the clinical development of drugs. Future studies using *in vivo* tumor models will evaluate the utility of such multi-targeting agents for overcoming the plasticity of cancer cell signaling networks that enable drug resistance.

Methods

Cell culture and chemical reagents. NIH3T3 and RMS13 cell lines were purchased from ATCC. *Ptch1*^{-/-} MEFs and 3T3-ShhFL cell lines were previously described²². SAHA was purchased from Cayman Chemical (#10009929). All other compounds were synthesized at UT Southwestern (see below).

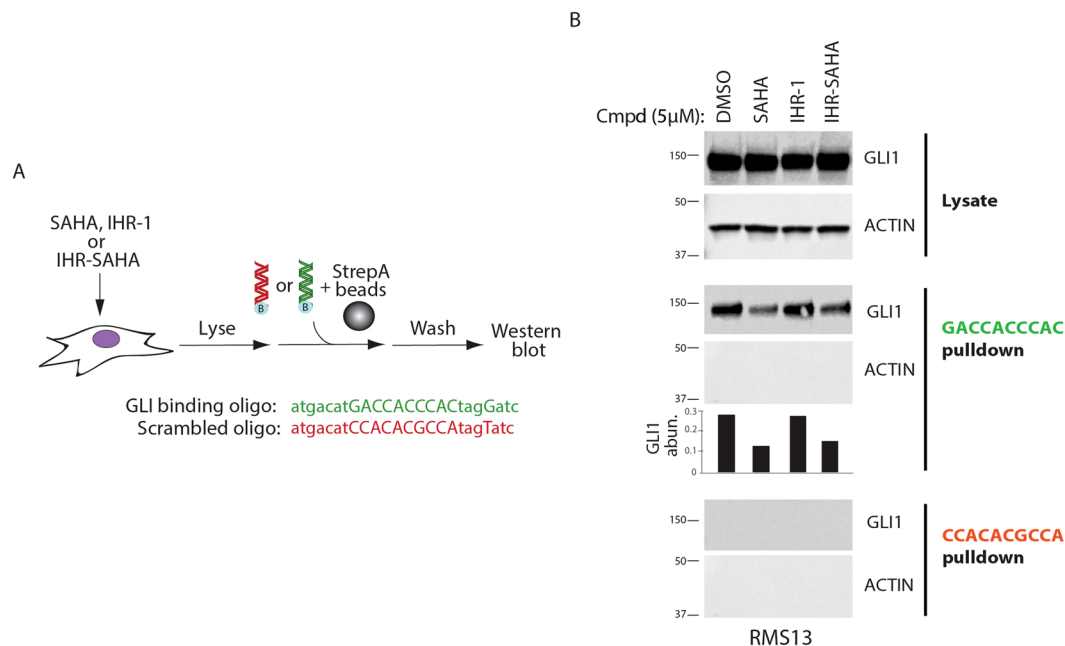


Figure 6. IHR-SAHA blocks GLI binding to DNA. **(A)** A biochemical assay for monitoring GLI interaction with DNA. Lysate from a cell line expressing a GLI protein is incubated with biotinylated oligos encoding either a consensus GLI binding motif or a scrambled sequence. The abundance of GLI binding to DNA is determined by Western blot analysis of material associated with oligo-bound streptavidin sepharose. **(B)** SAHA and IHR-SAHA decrease GLI binding to DNA. Lysate from RMS13 cells treated with indicated compounds were subjected to the assay described in **(A)** “GACCACCCAC” (green) is a GLI binding site oligonucleotide whereas “CCACACGCCA” (red) is a scrambled binding site oligonucleotide. The abundance of GLI1 bound to DNA was quantified. Unprocessed blots are found in Supplementary Fig. S3. Two independent experiments were performed.

Chemical synthesis. *Synthesis of IHR-SAHA.* A solution of *tert*-butyl (4-chloro-3-((4-(2,5-dichlorobenzamido)phenyl)carbamoyl)phenyl)carbamate²² (2.0 g, 3.7 mmol) in trifluoroacetic acid/dichloromethane (20% v/v, 6 mL) was stirred at 23 °C for 20 min. The volatiles were then removed and the residue purified by silica gel column chromatography (ethyl acetate/hexanes = 1/2 to 1/1) to give 5-amino-2-chloro-*N*-(4-(2,5-dichlorobenzamido)phenyl)benzamide as a yellow solid (1.5 g, 93% yield). ¹H NMR (500 MHz, DMSO-*d*₆) δ 10.58 (s, 1H), 10.39 (s, 1H), 7.75 (d, *J* = 2.3 Hz, 1H), 7.68 (q, *J* = 8.7 Hz, 6H), 7.64–7.59 (m, 3H), 7.14 (d, *J* = 8.6 Hz, 1H), 6.70 (d, *J* = 2.7 Hz, 1H), 6.65 (dd, *J* = 8.6, 2.6 Hz, 1H), 5.49 (brs, 2H). MS (ESI)⁺ calcd for C₂₀H₁₄Cl₃N₃O₂ [M + H]⁺ 434.0, found 434.0.

To a solution of monomethyl suberate (0.67 g, 3.63 mmol) in a mixture of dichloromethane (9 mL) and *N,N*-dimethylformamide (0.1 mL) was added oxalyl chloride (0.37 mL, 4.36 mmol) at 0 °C. After stirring at 23 °C for 10 min, a mixture of 5-amino-2-chloro-*N*-(4-(2,5-dichlorobenzamido)phenyl)benzamide (1.5 g, 3.45 mmol) and triethylamine (1.52 mL, 10.9 mmol) in dichloromethane (3 mL) was added and the solution was stirred at 23 °C for 3 h. After removing the volatiles, the residue was dissolved in methanol (12 mL) and aqueous hydroxylamine (50%, 1.2 mL). The solution was stirred at 60 °C for 16 h before concentrated and triturated with ethyl acetate/hexanes (1/1, 20 mL) to give IHR-SAHA as a white solid (1.0 g, 48% yield). ¹H NMR (500 MHz, DMSO-*d*₆) δ 10.60 (s, 1H), 10.53 (s, 1H), 10.35 (s, 1H), 10.19 (s, 1H), 8.69 (brs, 1H), 7.84 (d, *J* = 2.5 Hz, 1H), 7.76 (d, *J* = 2.3 Hz, 1H), 7.74–7.66 (m, 5H), 7.66–7.57 (m, 2H), 7.49 (d, *J* = 8.7 Hz, 1H), 2.33 (t, *J* = 7.3 Hz, 2H), 1.94 (t, *J* = 7.3 Hz, 2H), 1.63–1.55 (m, 2H), 1.52–1.46 (m, 2H), 1.35–1.22 (m, 4H). MS (ESI)⁺ calcd for C₂₈H₂₇Cl₃N₄O₆ [M + H]⁺ 605.1, found 605.0.

Synthesis of IHR (meta)-SAHA. A solution of *tert*-butyl (4-chloro-3-((3-(2,5-dichlorobenzamido)phenyl)carbamoyl)phenyl)carbamate²² (3.1 g, 6.2 mmol) in trifluoroacetic acid/dichloromethane (20% v/v, 20 mL) was stirred at 23 °C for 20 min. The volatiles were then removed and the residue purified by silica gel column chromatography (ethyl acetate/hexanes = 1/2 to 1/1) to give 5-amino-2-chloro-*N*-(3-(2,5-dichlorobenzamido)phenyl)benzamide as a yellow solid (1.6 g, 59% yield). ¹H NMR (400 MHz, DMSO-*d*₆) δ 10.61 (s, 1H), 10.42 (s, 1H), 8.16 (t, *J* = 2.1 Hz, 1H), 7.79–7.67 (m, 1H), 7.65–7.52 (m, 2H), 7.43 (d, *J* = 7.9 Hz, 1H), 7.41–7.35 (m, 1H), 7.28 (d, *J* = 7.9 Hz, 1H), 7.10 (d, *J* = 8.4 Hz, 1H), 6.74–6.58 (m, 2H), 5.44 (brs, 2H). MS (ESI)⁺ calcd for C₂₀H₁₄Cl₃N₃O₂ [M + H]⁺ 434.0, found 434.0.

To a solution of monomethyl suberate (0.53 g, 2.81 mmol) in a mixture of dichloromethane (20 mL) and *N,N*-dimethylformamide (0.1 mL) was added oxalyl chloride (0.3 mL, 3.37 mmol) at 0 °C. After stirring for 10 min at 23 °C, a mixture of 5-amino-2-chloro-*N*-(3-(2,5-dichlorobenzamido)phenyl)benzamide (1.11 g, 2.56 mmol) and triethylamine (1.18 mL, 8.43 mmol) in dichloromethane (10 mL) was added and the solution was stirred at

23 °C for 3 h. After removing the volatiles, the residue was dissolved in methanol (10 mL) and aqueous hydroxylamine (50%, 1.7 mL). The solution was stirred at 60 °C for 16 h before concentrated and triturated with ethyl acetate/hexanes (1/1, 15 mL) to give IHR (meta)-SAHA as a yellow solid (420 mg, 27% yield). ¹H NMR (400 MHz, DMSO-*d*₆) δ 10.63 (s, 1H), 10.56 (s, 1H), 10.35 (s, 1H), 10.17 (s, 1H), 8.78–8.59 (m, 1H), 8.27–8.08 (m, 1H), 7.78 (d, *J* = 2.5 Hz, 1H), 7.73–7.62 (m, 2H), 7.56 (d, *J* = 4.2 Hz, 2H), 7.42 (dd, *J* = 14.9, 8.1 Hz, 3H), 7.30 (t, *J* = 8.0 Hz, 1H), 2.28 (t, *J* = 6.9 Hz, 2H), 1.91 (t, *J* = 6.8 Hz, 2H), 1.54 (m, 2H), 1.46 (m, 2H), 1.24 (m, 4H). MS (ESI)⁺ calcd for C₂₈H₂₇Cl₃N₄O₆ [M + H]⁺ 605.1, found 605.0.

In vitro HDAC profiling. HDAC profiling was performed at BPS Bioscience (San Diego, CA). All of the compounds are dissolved in DMSO. A series of dilutions of the compounds were prepared with 10% DMSO in HDAC assay buffer (#50031) and 5 μl of the dilution was added to a 50 μl reaction so that the final concentration of DMSO is 1% in all of reactions. All of the enzymatic reactions were conducted in duplicate at 37 °C for 30 mins, except that the enzyme reactions for HDAC11 were at room temperature for 3 hrs. All of the reactions were performed in a 50 μl mixture containing HDAC assay buffer, 5 μg BSA, an HDAC substrate [HDAC Substrate 3 (BPS number 50037) or HDAC Class 2a Substrate 1 (BPS number 50040)], an HDAC enzyme (#50051-11) and a test compound. After enzymatic reactions, 50 μl of HDAC Developer (#50030) was added to each well and the plate was incubated at room temperature for an additional 20 mins. Fluorescence intensity was measured at an excitation of 360 nm and an emission of 460 nm using a Tecan Infinite M1000 microplate reader. HDAC activity assays were performed in duplicates at each concentration. The fluorescent intensity data were analyzed using the computer software, Graphpad Prism. In the absence of the compound, the fluorescent intensity (Ft) in each data set was defined as 100% activity. In the absence of HDAC, the fluorescent intensity (Fb) in each data set was defined as 0% activity. The percent activity in the presence of each compound was calculated according to the following equation: %activity = (F – Fb)/(Ft – Fb), where F = the fluorescent intensity in the presence of the compound. The values of % activity versus a series of compound concentrations were then plotted using non-linear regression analysis of Sigmoidal dose-response curve generated with the equation $Y = B + (T - B) / (1 + 10((\text{LogI} C50 - X) \times \text{Hill Slope}))$, where Y = percent activity, B = minimum percent activity, T = maximum percent activity, X = logarithm of compound and Hill Slope = slope factor or Hill coefficient. The IC₅₀ value was determined by the concentration causing a half-maximal percent activity. SAHA IC₅₀ data for individual HDACs was previously generated by BPS using similar assay conditions.

Reporter assay. The HH-responsive firefly luciferase reporter (GLI-BS) and a control *Renilla* luciferase reporter (SV40-RL) were transfected into indicated cell lines using Effectene (Qiagen) either alone or with indicated DNAs. 24 hrs after transfection, cells were switched to low serum media (3% calf serum), and grown for another 48 hrs. in 5% CO₂ in the presence/absence of compounds. 3T3-ShhFL cell line that stably expressing SHH and the two reporters were cultured in a similar fashion. FL and RL activities in lysate generated using Passive Lysis Buffer (Promega) were then assessed using the Dual-Luciferase kit (Promega) and a 96-well plate reading luminometer (BMG). The ratio of FL/RL was calculated and the averaged ratios from three replicates were reported.

Acetylation assay. For analyzing acetylation status of histone 3 and tubulin, NIH3T3 cells were grown to confluence in 6-well plates. After 48hrs of treatment with indicated chemicals, cells were lysed in RIPA buffer or 1% NP40/phosphate buffered saline/protease inhibitors (SIGMA, #S8820), the lysate cleared using a microcentrifuge, then 6 × sample loading buffer (BioLand Scientific) added to the supernatant. Proteins were separated on SDS-PAGE (BioRad Criterion TGX Precast Gels). Antibodies used for analyzing the blots were: acetylated tubulin (SIGMA, #T6793), tubulin, acetyl-histone H3 (Lys23), and histone H3 (Cell Signaling Technology, #2125 S, #8848 and #9717, respectively). Chemiluminescence was detected using a Li-COR Odyssey Imaging System.

GLI DNA binding assay. A detailed protocol for DNA binding assay was previously described⁴¹. Briefly, cells treated for 48 hrs with compounds were lysed in 1% NP40/phosphate buffered saline/protease inhibitors and cleared using a microcentrifuge. The lysate was then incubated with 0.5 μM of double-strand biotinylated oligonucleotides and 40 μl streptavidin-agarose bead suspension (Thermo Scientific, 20349) for 2 hrs. The streptavidin agarose beads are washed (3X) with 1% NP40/phosphate buffered saline/protease inhibitors and eluted with 2X Laemmli sample buffer. The supernatants are separated on SDS-PAGE and analyzed using western blotting. Antibodies were purchased from the following vendors: GLI1 (Cell Signaling Technology, #2534) and actin (SIGMA, #A5441).

Compound cellular permeability. Caco-2 cell permeability assay was previously described²². Briefly, Caco-2 cells were grown to confluence in 12-well transwell plates. Culture medium was replaced with 10 μM of compounds in DMEM/ 3% calf serum and incubated for 6hrs. Media from the top and bottom chamber were collected and diluted in DMEM/ 3% calf serum as indicated in the figure. Diluted media were added to confluent 3T3-ShhFL cells for 48hrs and measure the Hh pathway activity by reporter assay.

Data availability. All data generated or analyzed during this study are included in this published article (and its Supplementary Information files).

References

- Jiang, J. & Hui, C. C. Hedgehog signaling in development and cancer. *Dev Cell* **15**, 801–812 (2008).
- Humke, E. W., Dorn, K. V., Milenkovic, L., Scott, M. P. & Rohatgi, R. The output of Hedgehog signaling is controlled by the dynamic association between Suppressor of Fused and the Gli proteins. *Genes Dev* **24**, 670–682 (2010).
- Tukachinsky, H., Lopez, L. V. & Salic, A. A mechanism for vertebrate Hedgehog signaling: recruitment to cilia and dissociation of SuFu-Gli protein complexes. *J Cell Biol* **191**, 415–428 (2010).

4. Bonilla, X. *et al.* Genomic analysis identifies new drivers and progression pathways in skin basal cell carcinoma. *Nat Genet* **48**(4), 398–406 (2016).
5. Kool, M. *et al.* Genome sequencing of SHH medulloblastoma predicts genotype-related response to smoothed inhibition. *Cancer Cell* **25**, 393–405 (2014).
6. Sekulic, A. & Von Hoff, D. Hedgehog Pathway Inhibition. *Cell* **164**, 831 (2016).
7. Brinkhuizen, T. *et al.* Acquired resistance to the Hedgehog pathway inhibitor vismodegib due to smoothed mutations in treatment of locally advanced basal cell carcinoma. *J Am Acad Dermatol* **71**, 1005–1008 (2014).
8. Dijkgraaf, G. J. *et al.* Small molecule inhibition of GDC-0449 refractory smoothed mutants and downstream mechanisms of drug resistance. *Cancer Res* **71**, 435–444 (2011).
9. Pricl, S. *et al.* Smoothened (SMO) receptor mutations dictate resistance to vismodegib in basal cell carcinoma. *Mol Oncol* **9**, 389–397 (2015).
10. Wang, C. *et al.* Structural basis for Smoothened receptor modulation and chemoresistance to anticancer drugs. *Nature communications* **5**, 4355 (2014).
11. Yauch, R. L. *et al.* Smoothened mutation confers resistance to a Hedgehog pathway inhibitor in medulloblastoma. *Science* **326**, 572–574 (2009).
12. Atwood, S. X., Li, M., Lee, A., Tang, J. Y. & Oro, A. E. GLI activation by atypical protein kinase C iota/lambda regulates the growth of basal cell carcinomas. *Nature* **494**, 484–488 (2013).
13. Buonamici, S. *et al.* Interfering with resistance to smoothed antagonists by inhibition of the PI3K pathway in medulloblastoma. *Sci Transl Med* **2** (2010).
14. Sharpe, H. J. *et al.* Genomic analysis of smoothed inhibitor resistance in basal cell carcinoma. *Cancer Cell* **27**, 327–341 (2015).
15. Beauchamp, E. M. *et al.* Arsenic trioxide inhibits human cancer cell growth and tumor development in mice by blocking Hedgehog/GLI pathway. *J Clin Invest* **121**, 148–160 (2011).
16. Kim, J., Lee, J. J., Gardner, D. & Beachy, P. A. Arsenic antagonizes the Hedgehog pathway by preventing ciliary accumulation and reducing stability of the Gli2 transcriptional effector. *Proc Natl Acad Sci USA* **107**, 13432–13437 (2010).
17. Agyeman, A., Jha, B. K., Mazumdar, T. & Houghton, J. A. Mode and specificity of binding of the small molecule GANT61 to GLI determines inhibition of GLI-DNA binding. *Oncotarget* **5**, 4492–4503 (2014).
18. Wu, X. *et al.* Rac1 activation controls nuclear localization of beta-catenin during canonical Wnt signaling. *Cell* **133**, 340–353 (2008).
19. Hyman, J. M. *et al.* Small-molecule inhibitors reveal multiple strategies for Hedgehog pathway blockade. *Proc Natl Acad Sci USA* **106**, 14132–14137 (2009).
20. Canetti, G. *et al.* Histone deacetylase and Cullin3-REN(KCTD11) ubiquitin ligase interplay regulates Hedgehog signalling through Gli acetylation. *Nat Cell Biol* **12**, 132–142 (2010).
21. Coni, S. *et al.* Selective targeting of HDAC1/2 elicits anticancer effects through Gli1 acetylation in preclinical models of SHH Medulloblastoma. *Sci Rep* **7**, 44079 (2017).
22. Fan, C. W. *et al.* The Hedgehog pathway effector smoothed exhibits signaling competency in the absence of ciliary accumulation. *Chem Biol* **21**, 1680–1689 (2014).
23. Atadja, P. Development of the pan-DAC inhibitor panobinostat (LBH589): successes and challenges. *Cancer Lett* **280**, 233–241 (2009).
24. Marks, P. A. & Breslow, R. Dimethyl sulfoxide to vorinostat: development of this histone deacetylase inhibitor as an anticancer drug. *Nature biotechnology* **25**, 84–90 (2007).
25. Taipale, J. *et al.* Effects of oncogenic mutations in Smoothened and Patched can be reversed by cyclopamine. *Nature* **406**, 1005–1009 (2000).
26. Hubbert, C. *et al.* HDAC6 is a microtubule-associated deacetylase. *Nature* **417**, 455–458 (2002).
27. Matsuyama, A. *et al.* *In vivo* destabilization of dynamic microtubules by HDAC6-mediated deacetylation. *EMBO J* **21**, 6820–6831 (2002).
28. Filbin, M. G. *et al.* Coordinate activation of Shh and PI3K signaling in PTEN-deficient glioblastoma: new therapeutic opportunities. *Nature medicine* **19**, 1518–1523 (2013).
29. Kasiri, S. *et al.* GLI1 Blockade Potentiates the Antitumor Activity of PI3K Antagonists in Lung Squamous Cell Carcinoma. *Cancer Res* **77**, 4448–4459 (2017).
30. Zhao, J., Quan, H., Xie, C. & Lou, L. NL-103, a novel dual-targeted inhibitor of histone deacetylases and hedgehog pathway, effectively overcomes vismodegib resistance conferred by Smo mutations. *Pharmacol Res Perspect* **2**, e00043 (2014).
31. Chun, S. G. *et al.* Targeted inhibition of histone deacetylases and hedgehog signaling suppress tumor growth and homologous recombination in aerodigestive cancers. *Am J Cancer Res* **5**, 1337–1352 (2015).
32. Chun, P. Histone deacetylase inhibitors in hematological malignancies and solid tumors. *Arch Pharm Res* **38**, 933–949 (2015).
33. Dhanyamraju, P. K., Holz, P. S., Finkernagel, F., Fendrich, V. & Lauth, M. Histone deacetylase 6 represents a novel drug target in the oncogenic Hedgehog signaling pathway. *Molecular cancer therapeutics* **14**, 727–739 (2015).
34. Zhang, Z. *et al.* Suppressor of Fused Chaperones Gli Proteins To Generate Transcriptional Responses to Sonic Hedgehog Signaling. *Mol Cell Biol* **37** (2017).
35. Ehnert, S. *et al.* TGF-beta1 impairs mechanosensation of human osteoblasts via HDAC6-mediated shortening and distortion of primary cilia. *J Mol Med (Berl)* **95**, 653–663 (2017).
36. Goetz, S. C., Ocbina, P. J. & Anderson, K. V. The primary cilium as a Hedgehog signal transduction machine. *Methods in cell biology* **94**, 199–222 (2009).
37. Gradilone, S. A. *et al.* HDAC6 inhibition restores ciliary expression and decreases tumor growth. *Cancer Res* **73**, 2259–2270 (2013).
38. Jacob, L. S. *et al.* Genome-wide RNAi screen reveals disease-associated genes that are common to Hedgehog and Wnt signaling. *Science signaling* **4**, ra4 (2011).
39. Xiang, W. *et al.* HDAC6 inhibition suppresses chondrosarcoma by restoring the expression of primary cilia. *Oncology reports* **38**, 229–236 (2017).
40. Paller, C. J. *et al.* Design of phase I combination trials: recommendations of the Clinical Trial Design Task Force of the NCI Investigational Drug Steering Committee. *Clin Cancer Res* **20**, 4210–4217 (2014).
41. Wu, K. K. Analysis of protein-DNA binding by streptavidin-agarose pull-down. *Methods in molecular biology (Clifton, N.J)* **338**, 281–290 (2006).

Acknowledgements

This work was supported in part by the Welch Foundation (I-1665, L.L. and I-1868, C.C.), and CPRIT (RP130212, L.L. and C.C.) and the American Cancer Society (RSG-16-090-01-TBG, J.K.). Research reported in this publication was supported by the National Cancer Institute of the National Institutes of Health under Award Number R01CA168761 (J.K.), R01CA196851 (J.K.), and P50-CA70907 (Minna). The content is solely the responsibility of the authors and does not necessarily represent the official views of the National Institutes of Health.

Author Contributions

Conceived and designed the experiments: C.-W. F., N.Y., H.S., O.K., and L.L. Performed the experiments: C.-W. F., N.Y., H.S., O.K., L.L. Analyzed the data: C.-W. F., N.Y., J.K., L.L., C.C. Wrote the paper: J.K., C.C., L.L.

Additional Information

Supplementary information accompanies this paper at <https://doi.org/10.1038/s41598-018-19408-9>.

Competing Interests: The authors declare that they have no competing interests.

Publisher's note: Springer Nature remains neutral with regard to jurisdictional claims in published maps and institutional affiliations.



Open Access This article is licensed under a Creative Commons Attribution 4.0 International License, which permits use, sharing, adaptation, distribution and reproduction in any medium or format, as long as you give appropriate credit to the original author(s) and the source, provide a link to the Creative Commons license, and indicate if changes were made. The images or other third party material in this article are included in the article's Creative Commons license, unless indicated otherwise in a credit line to the material. If material is not included in the article's Creative Commons license and your intended use is not permitted by statutory regulation or exceeds the permitted use, you will need to obtain permission directly from the copyright holder. To view a copy of this license, visit <http://creativecommons.org/licenses/by/4.0/>.

© The Author(s) 2018